

Article

Microstructure, Mechanical Properties, and Fish-Scaling Resistance of a Ti-Nb Microalloyed Hot-Rolled Enamel Steel

Yi Zhang^{1,2,*}, Bo Yu², Jian Zhang², Yu Du³, Xiaonan Wang³, Hongyan Wu¹, Xiuhua Gao¹ and Linxiu Du¹¹ State Key Laboratory of Rolling and Automation, Northeastern University, Shenyang 110819, China² Technology Center, Ma'anshan Iron & Steel Co., Ltd., Ma'anshan 243000, China³ School of Iron and Steel, Soochow University, Suzhou 215021, China

* Correspondence: mgzwx@163.com

Abstract: Currently, the fish-scaling resistance of most hot-rolled enamel steels is improved by adding Ti to form fine TiC carbides as hydrogen traps. Given that the hydrogen capture capacity of NbC is higher than that of TiC, the manufacture of hot-rolled enamel steels via Ti-Nb microalloying has a promising future. In the present study, a Ti-Nb microalloyed hot-rolled enamel steel was developed, and its microstructure, mechanical properties, and fish-scaling resistance were studied by optical microscopy, transmission electron microscopy, tensile test, and hydrogen permeation test. The results show that the microstructure of hot-rolled experimental steel is composed of ferrite and fine carbides, with a large number of fine precipitates uniformly distributed in the ferrite grains. After the first and second enamel firings, the average sizes of ferrite grain and precipitates gradually increase, the yield strength decreases from 711 ± 9 MPa to 471 ± 17 MPa and 409 ± 8 MPa, the tensile strength decreases from 761 ± 7 MPa to 524 ± 15 MPa and 490 ± 12 MPa, and the elongation increases from $21.0 \pm 2.8\%$ to $27.8 \pm 1.8\%$ and $33.9 \pm 1.1\%$. The hydrogen permeation value (*TH* value) decreases from 35.9 min/mm^2 to 6.8 min/mm^2 and 3.9 min/mm^2 after the first and second enamel firings. That is, the fish-scaling resistance of hot-rolled experimental steel is significantly reduced after enamel firing, which is caused by the coarsening of precipitates, resulting in a significant reduction in the density of irreversible hydrogen traps (from $1.21 \times 10^{25} \text{ cm}^{-3}$ to $6.50 \times 10^{23} \text{ cm}^{-3}$ and $4.27 \times 10^{23} \text{ cm}^{-3}$). A large amount of semi-coherent precipitates is the key to obtaining the good fish-scaling resistance of hot-rolled enamel steel.

Keywords: hot-rolled enamel steel; microstructure; fish-scaling resistance; hydrogen permeation test; irreversible hydrogen trap



Citation: Zhang, Y.; Yu, B.; Zhang, J.; Du, Y.; Wang, X.; Wu, H.; Gao, X.; Du, L. Microstructure, Mechanical Properties, and Fish-Scaling Resistance of a Ti-Nb Microalloyed Hot-Rolled Enamel Steel. *Metals* **2022**, *12*, 1970. <https://doi.org/10.3390/met12111970>

Academic Editor: Beatriz López Soria

Received: 25 October 2022

Accepted: 14 November 2022

Published: 18 November 2022

Publisher's Note: MDPI stays neutral with regard to jurisdictional claims in published maps and institutional affiliations.



Copyright: © 2022 by the authors. Licensee MDPI, Basel, Switzerland. This article is an open access article distributed under the terms and conditions of the Creative Commons Attribution (CC BY) license (<https://creativecommons.org/licenses/by/4.0/>).

1. Introduction

Enameled products combine the high strength and formability of steel matrix with the high temperature, acid, and alkali resistance as well as ease of cleaning of enamel coating [1,2], and have been widely used in applications requiring corrosion and high-temperature resistance, such as oven liners, water heater liners, sewage treatment facilities, etc. Enamel steel can be divided into cold-rolled enamel steel and hot-rolled enamel steel based on the production process. Cold-rolled enamel steel has good formability and is often used for enameled products requiring high formability [3]. Compared with cold-rolled enamel steel, hot-rolled enamel steel has higher strength and thickness and is usually used to produce some structural components, such as enamel assembling tanks for sewage treatment facilities [4,5]. In the production of enamel assembling tanks, the hot rolled enamel steel plate is first bent and then enamel fired twice. The first enamel firing is for the precoat [6], which is fired at ~ 890 °C. The second enamel firing is for the top coat, which is fired at ~ 860 °C. From the viewpoint of structural design, the yield strength of the hot-rolled enamel steel after two enamel firings should be higher than a specified value. In addition, the hot-rolled enamel steel should have excellent fish-scaling resistance to prevent the occurrence of fish-scaling.

Fish-scaling is a common and dangerous defect of enameled products, which refers to the phenomenon that the enamel coating of enameled products peels off. During the enamel firing process, hydrogen is dissolved in the austenite matrix and then diffuses from the steel matrix to the steel-enamel interface upon cooling due to a sharp decrease in solubility [7]. When the pressure generated by the hydrogen accumulated at the interface is greater than the bonding strength of the enamel coating and the steel matrix, the enamel layer will fall off, which is the cause of the fish-scaling. That is, the fish-scaling phenomenon is closely related to the diffusible hydrogen atoms in enamel steel [7,8]. Optimizing the chemical composition and production process to increase the number of hydrogen traps in steel is the main method to improve the fish-scaling resistance [5,9,10]. Theoretically, TiC, NbC, and VC precipitates can be used as hydrogen traps to improve the fish-scaling resistance of enamel steel. It has been found that the broad interface between TiC carbides and steel matrix was the main trapping site [11,12]. Therefore, reducing the size of TiC to increase its surface area is a way to increase the number of hydrogen traps. It is generally believed that the semi-coherent NbC precipitates trap hydrogen during cathodic charging at room temperature [13]. Recently, Chen et al. [14] observed that the incoherent interface between niobium carbides and steel matrix can act as a hydrogen trapping site, which provides a new perspective to improve the fish-scaling resistance. Shi et al. [15] also found that incoherent NbC can be used as a hydrogen trap to inhibit hydrogen accumulation. The hydrogen-trapping sites for TiC and NbC are generally considered to be the misfit dislocation core at the interface [16,17]. Unlike TiC and NbC carbides, the hydrogen trapping site of the VC precipitates is the carbon vacancy on the (001) coherent surface [18]. Turk et al. [19] found that smaller VC precipitates trapped more hydrogen, suggesting that the trapping is surface-dominant. At present, the fish-scaling resistance of hot-rolled enamel steel is increased mainly by adding Ti to form a large number of fine TiC precipitates as hydrogen traps. Huang et al. [4] and Zhao et al. [5] have investigated the fish-scaling resistance of hot-rolled enamel steel by hydrogen permeation tests. They both found that the fish-scaling resistance increased as the size of TiC precipitates decreased. This is because the hydrogen atoms were mainly trapped at the TiC/ferrite interface [11,12], and the decrease in TiC particle size resulted in an increase in the interface area, which led to an increase in the number of hydrogen traps. Considering that the hydrogen capture capacity of NbC is higher than that of TiC [20], it is feasible to produce hot-rolled enamel steel via Ti-Nb microalloying, but there are few studies on Ti-Nb microalloyed hot-rolled enamel steel. To promote the development of Ti-Nb microalloyed hot-rolled enamel steel and reveal the effect of hydrogen traps on the fish-scaling resistance, it is necessary to investigate the relationship among microstructure, mechanical properties, and fish-scaling resistance.

At present, the fish-scaling resistance of enamel steel is usually evaluated by the hydrogen permeation test with one hydrogen-charging process. This method cannot quantitatively evaluate the effect of hydrogen trap density on the fish-scaling resistance. Considering that the fish-scaling resistance of enamel steel is highly dependent on the hydrogen trap density, it is necessary to determine the hydrogen trap density experimentally. Zhou et al. [21] pointed out that the total hydrogen trap density and irreversible hydrogen trap density can be obtained using a hydrogen permeation test with two hydrogen-charging processes. In this paper, we will use the above method to determine the hydrogen trap density in enamel steel and further explore the relationship between hydrogen trap density and fish-scaling resistance.

2. Materials and Methods

The experimental material is a Ti-Nb microalloyed hot-rolled enamel steel, and its chemical composition is listed in Table 1. After smelting, the experimental steel was cast into a slab with a thickness of 230 mm. The slab was hot rolled into a strip with a thickness of 5 mm at a finish rolling temperature of 880 °C after austenitizing at 1250 °C and holding for 2 h. After finishing rolling, the strip was laminar cooled to 640 °C and slowly cooled to room temperature. In order to study the microstructure and properties of the experimental

steel after the first and second enamel firings, the hot-rolled steel strips were subjected to simulated enamel firing. The steel strip was heated to 890 °C and held for 10 min during the first simulated enamel firing, and then air-cooled to room temperature. The temperature and holding time of the second simulated enamel firing were 860 °C and 10 min. After the second simulated enamel firing, the steel strip was cooled to room temperature. For the convenience of expression, the hot-rolled experimental steel and the steels after the first and second simulated enamel firing were denoted as HR, EF1, and EF2 samples, respectively.

Table 1. Chemical composition of the Ti-Nb microalloyed hot-rolled enamel steel (wt.%).

C	Si	Mn	P	S	Als	Ti	Nb	N
0.042	0.0085	1.30	0.042	0.018	0.035	0.126	0.016	0.0017

Tensile specimens, metallographic specimens, and transmission electron microscopy (TEM) specimens were cut along the transverse direction of HR, EF1, and EF2 samples. The gauge length and width of the tensile specimen were 100 mm and 25 mm, respectively. The tensile test was carried out on a ZWICK 1200 kN tensile testing machine. Three tensile specimens were tested in each group and the mechanical properties results were the average values. The metallographic specimen was ground, polished, and etched with a 4 vol.% nital solution, and then observed by Axio M2m optical microscopy (OM). The size, morphology, and distribution of the second-phase precipitates were observed by FEI TECNAI G² F20 field emission TEM.

The hydrogen permeation experiment was carried out using a Fe-HP-12 hydrogen permeation tester at room temperature, which is based on the principle of the Devanathan–Stachurski double electrolysis cell [22,23]. Hydrogen permeation specimens were cut from the HR, EF1, and EF2 samples with cross-dimensions of 50 mm × 80 mm and the thickness of 2.59 mm, 1.95 mm, and 1.95 mm, respectively. The surface of the hydrogen permeation specimen was ground using 600# sandpaper and then cleaned with acetone. Prior to the hydrogen permeation test, the surface of the specimens on the hydrogen-releasing side was nickel coated to reduce the background current. The hydrogen permeation specimen was mounted between the hydrogen-charging cell and the hydrogen-releasing cell with a contact diameter of 3 cm (exposed area of 7.065 cm²). The hydrogen-releasing cell was filled with a 0.2 M NaOH aqueous solution, and a constant potential of 0.2 V was applied to remove the residual hydrogen from the specimen. When the background current in the hydrogen-releasing cell was less than 5 μA/cm², a 0.2 M NaOH solution was added to the hydrogen-charging cell and a current density of 3 mA/cm² was applied to the hydrogen charging cell. Furthermore, 1M of Na₂S was also added to the hydrogen-charging cell to prevent the recombination of hydrogen atoms into hydrogen molecules. The anode current and time were recorded during the experiment. Once the anode current in the hydrogen-releasing cell had reached a stable value, the charging current in the hydrogen-charging cell was removed and the first hydrogen permeation test was completed. The second hydrogen permeation process was then started using the same procedure when the background current was once more reduced to a stable value.

The following equations were used to calculate the hydrogen permeation parameters such as effective hydrogen diffusion coefficient (D_{eff}), total hydrogen trap density (N_{T}), irreversible hydrogen trap density (N_{ir}), reversible hydrogen trap density (N_{r}), and hydrogen permeation value (TH) [5,24–26].

$$D_{\text{eff}} = \frac{d^2}{6t_{0.63}} \quad (1)$$

$$N_{\text{T}} = N_{\text{L}} \times \left(\frac{D_{\text{L}}}{D_{\text{eff}}} - 1 \right) \times e^{-(E_{\text{b}}/RT)} \quad (2)$$

$$N_{\text{ir}} = N_{\text{T1}} - N_{\text{T2}} \quad (3)$$

$$N_{\text{r}} = N_{\text{T2}} \quad (4)$$

$$TH = t_b / d^2 \quad (5)$$

where d is the thickness of the hydrogen permeation specimen; $t_{0.63}$ is the lag time when $I = 0.63$ times the steady state current; N_{T1} and N_{T2} are the hydrogen trap densities for the first and second hydrogen permeation processes, respectively; $N_L = 7.52 \times 10^{22} \text{ cm}^{-3}$ [26]; $E_b = 0.3 \text{ eV}$ [26]; R is the gas constant, $8.314 \text{ J}\cdot\text{mol}^{-1}\cdot\text{K}^{-1}$; T is the absolute temperature; t_b is the hydrogen permeation time, and its determination method was described in Reference [5]. The lower the D_{eff} and the higher the TH , the better the fish-scaling resistance of enamel steel.

3. Results and Discussion

3.1. Microstructure

The OM microstructures of the HR, EF1, and EF2 samples are shown in Figure 1. It can be seen that the microstructures of the HR, EF1, and EF2 samples are all composed of ferrite (white matrix, as indicated by the red arrows) and fine carbides (as indicated by the black arrows). The average ferrite grain sizes of the HR, EF1, and EF2 samples are $3.21 \pm 0.24 \mu\text{m}$, $5.43 \pm 0.68 \mu\text{m}$, and $6.58 \pm 0.35 \mu\text{m}$, respectively, using the linear intercept method. It can be observed that the average ferrite grain size increases after the enamel firing, and the average ferrite grain size after the second enamel firing is larger than that after the first enamel firing. It can also be noticed that the shape of the ferrite grains changes from pancake to equiaxial after enamel firing.

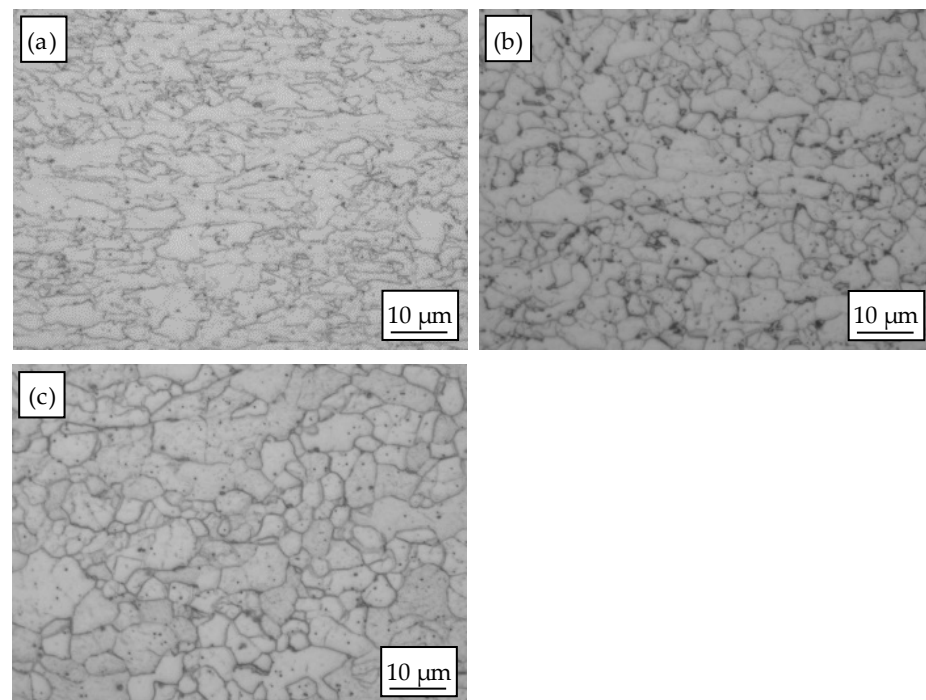


Figure 1. OM microstructures of different samples: (a) HR sample; (b) EF1 sample; (c) EF2 sample.

The typical morphology photos of precipitates in the HR, EF1, and EF2 samples are presented in Figure 2. It can be observed that the precipitates (small black particles, as indicated by the black arrows) are uniformly distributed in the ferrite grains (as indicated by the red arrows) in these three samples. The average sizes of the precipitates in the HR, EF1, and EF2 samples are measured using Image Pro Plus software to be 7.5 nm, 12.5 nm, and 13.5 nm, respectively. The effective sizes of precipitates were determined by their area. It can be found that the average of the precipitates gradually increases after enamel firing.

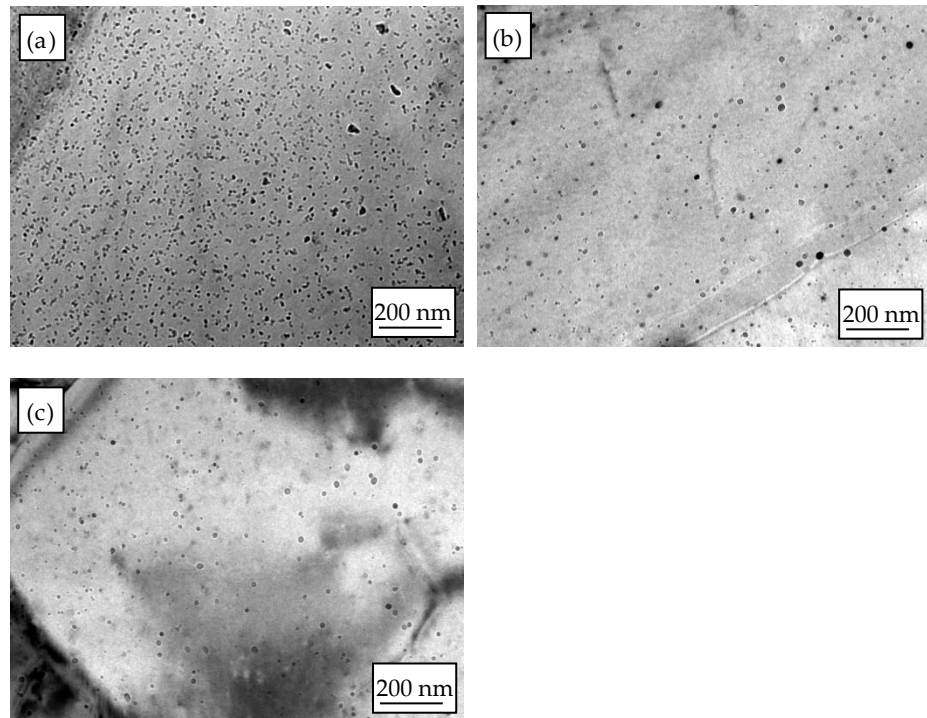


Figure 2. TEM images of precipitates in (a) HR sample; (b) EF1 sample; (c) EF2 sample.

The size distribution of the precipitates in the HR, EF1, and EF2 samples is displayed in Figure 3. In order to accurately measure the size of the precipitates, 10 TEM photos were taken for analysis of each sample. The number of analyzed precipitates in the HR, EF1, and EF2 samples was approximately 8300, 1600, and 1200, respectively. The relative frequency of the precipitates is largest when the precipitate size is 2–4 nm in the HR sample, and when the precipitate size was approximately 12–14 nm and 10–12 nm in the EF1 and EF2 samples.

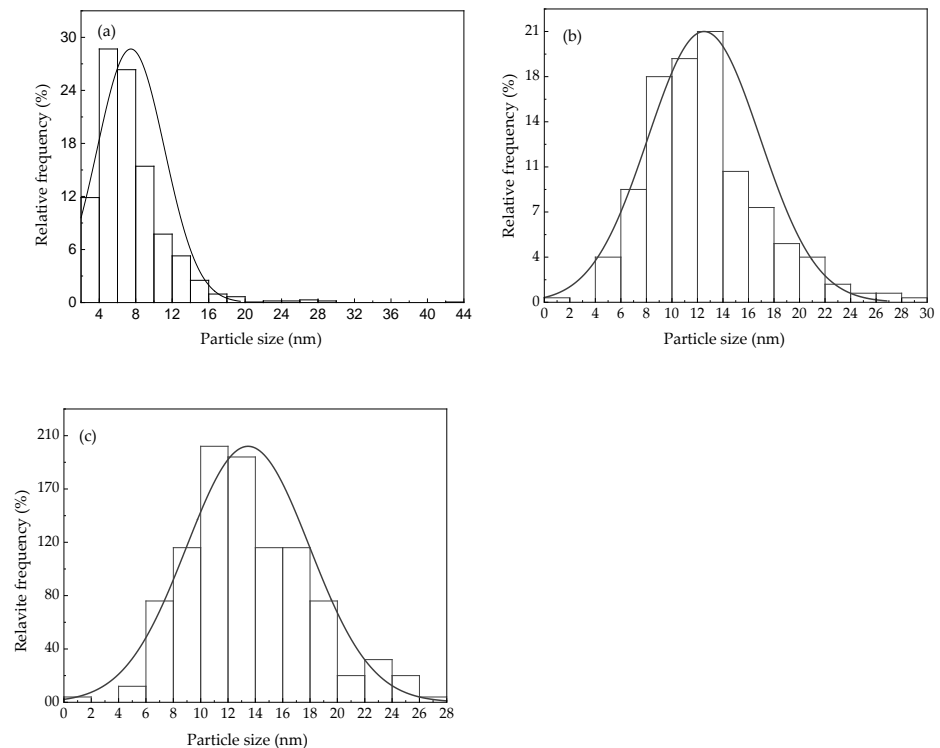


Figure 3. Size distribution of the precipitates in (a) HR sample; (b) EF1 sample; (c) EF2 sample.

3.2. Mechanical Properties

The mechanical properties of the HR, EF1, and EF2 samples are listed in Table 2. It can be seen that the HR sample has the highest yield strength and tensile strength, which are 711 ± 9 MPa and 761 ± 7 MPa, respectively. After the first and second enamel firings, the yield and tensile strength gradually decrease and the elongation gradually increases, which is consistent with the experimental results observed by Huang et al. [4]. After the second enamel firing, the yield and tensile strength are reduced to 409 MPa and 490 MPa, respectively.

Table 2. Mechanical properties of HR, EF1, and EF2 samples.

Sample	Yield Strength (MPa)	Tensile Strength (MPa)	Elongation (%)
HR	711 ± 9	761 ± 7	21.0 ± 2.8
EF1	471 ± 17	524 ± 15	27.8 ± 1.8
EF2	409 ± 8	490 ± 12	33.9 ± 1.1

It is evident that after the first and second enamel firing, the average ferrite grain size increases, and the average size of precipitates increases as well as the precipitate density decreases, which leads to a reduction in the contribution of fine grain strengthening and precipitation strengthening to the yield strength. In addition, the dislocation density can be reduced by the enamel firing, resulting in a reduction in dislocation strengthening. For example, Jiang et al. [27] investigated the change in dislocation density of hot-rolled enamel steel after enamel firing and found that the dislocation density decreased by 48%. The decrease in strength is therefore caused by an increase in the average ferrite grain size, an increase in the average size of precipitates, and a decrease in the dislocation density.

3.3. Hydrogen Permeation Parameters

The current–time ($I-t$) curves of the HR, EF1, and EF2 samples during the hydrogen permeation test are shown in Figure 4. The $t_{0.63}$ of the three specimens during the first and second hydrogen permeation experiments can be determined from Figure 4, and by substituting them into Equations (1)–(4), hydrogen permeation parameters such as D_{eff} , N_{T} , N_{ir} , and $N_{\text{ir}}/N_{\text{T}}$ can be obtained, and these parameters are listed in Table 3. By integrating the $I-t$ curve of the first hydrogen permeation test in Figure 4, the charge–time curve can be obtained, as shown in Figure 5. The t_{b} of the HR, EF1, and EF2 samples can be determined to be 240.5 min, 25.8 min, and 15.0 min, respectively, by using the method described in Reference [5]. According to Equation (5), the TH values of the HR, EF1, and EF2 samples can be calculated to be $35.9 \text{ min}\cdot\text{mm}^{-2}$, $6.8 \text{ min}\cdot\text{mm}^{-2}$, and $3.9 \text{ min}\cdot\text{mm}^{-2}$, respectively. The TH values of the three samples are also listed in Table 3.

As can be seen from Table 3, the HR sample has the lowest D_{eff} and the highest TH , which means that the hot-rolled experimental steel has the highest fish-scaling resistance. After the first and second enamel firings, D_{eff} gradually increases and TH gradually decreases, indicating a gradual decrease in the fish-scaling resistance. At present, the fish-scaling resistance of enamel steel is evaluated by a hydrogen permeation test, and there are mainly two evaluation parameters, D_{eff} and TH . It is generally believed that when D_{eff} is less than $2.0 \times 10^{-6} \text{ cm}^2\cdot\text{s}^{-1}$ [9] or TH is greater than $6.7 \text{ min}\cdot\text{mm}^{-2}$ [28], the fish-scaling will not occur after enamel firing. However, there is no conclusion about which parameter can better evaluate the fish-scaling resistance of enamel steel. Hydrogen traps can be divided into reversible and irreversible hydrogen traps according to the binding energy of hydrogen traps. Grain boundaries and dislocations are reversible hydrogen traps with low binding energy, and hydrogen can easily escape after being trapped by them. The precipitates are the main irreversible hydrogen traps in hot-rolled enamel steel, and their binding energy is high, making it difficult for trapped hydrogen to escape. Studies by Huang et al. [4] and Zhao et al. [5] on Ti-containing hot-rolled enamel steels both showed that TiC is an irreversible trap that significantly affects fish-scaling resistance. However,

their work was qualitative in analysis and did not quantitatively investigate the effect of total hydrogen trap density or irreversible hydrogen trap density on TH . Dong et al. [9] investigated the effect of B on D_{eff} in cold-rolled enamel steel and found that the addition of B reduced D_{eff} , but they also did not investigate the effect of total hydrogen trap density or irreversible hydrogen trap density on D_{eff} . The relationships between TH , D_{eff} and N_T , N_{ir} of the three samples are presented in Figure 6. It can be seen from Figure 6 that only TH and N_T have a good linear relationship, which suggests that it is reasonable to use TH to characterize the fish-scaling resistance of enamel steel.

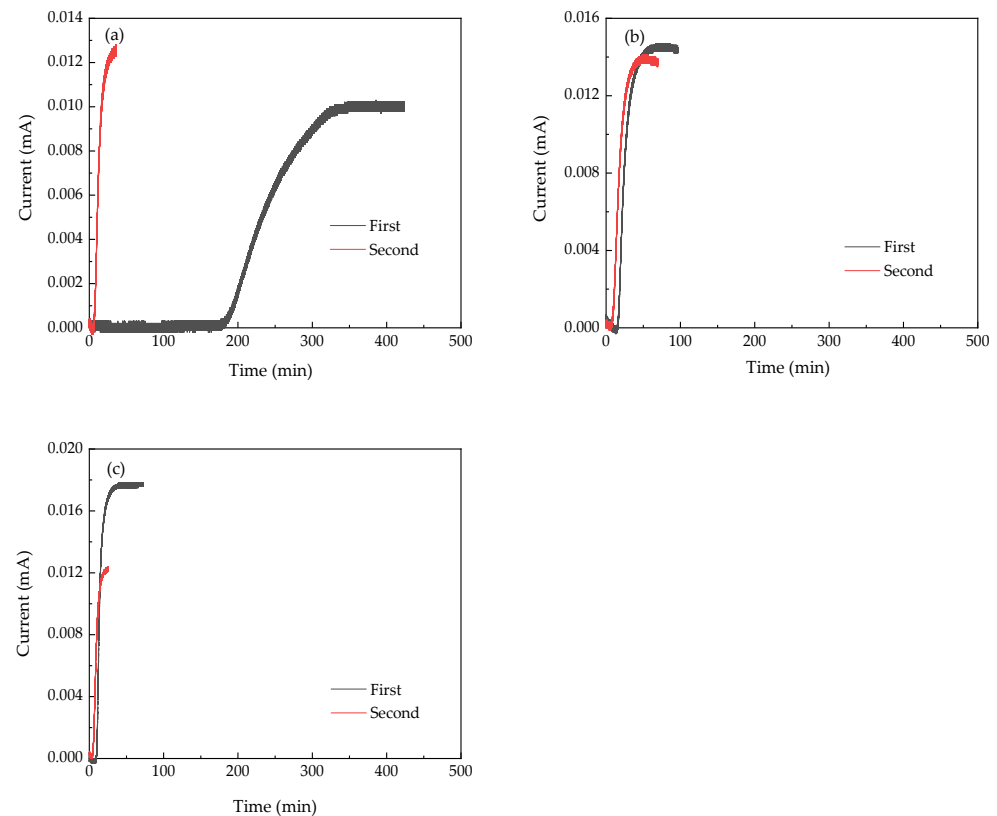


Figure 4. Current–time curves of hydrogen permeation test: (a) HR sample; (b) EF1 sample; (c) EF2 sample.

Table 3. Hydrogen permeation parameters of HR, EF1, and EF2 samples.

Sample	D_{eff} ($\text{cm}^2 \cdot \text{s}^{-1}$)	N_T (cm^{-3})	N_{ir} (cm^{-3})	N_{ir}/N_r	TH ($\text{min} \cdot \text{mm}^{-2}$)
HR	7.52×10^{-7}	1.27×10^{25}	1.21×10^{25}	0.95	35.9
EF1	4.08×10^{-6}	2.29×10^{24}	6.50×10^{23}	0.28	6.8
EF2	7.31×10^{-6}	1.24×10^{24}	4.27×10^{23}	0.34	3.9

It can be seen from Table 3 that the N_{ir}/N_T of the HR sample is 0.95, which indicates that most hydrogen traps in the HR sample are irreversible hydrogen traps. The density of irreversible hydrogen traps decreases sharply after the first and second enamel firings, while the density of reversible hydrogen traps does not change much, so it can be concluded that the reduction of fish-scaling resistance after enamel firing is mainly caused by the decrease in irreversible hydrogen trap density. The precipitates are the main irreversible hydrogen traps in hot-rolled enamel steel. As can be seen from Table 3 and Figure 6, the density of irreversible hydrogen traps decreases significantly as the average size of the precipitates increases from 7.5 nm to 12.5 nm. Wei et al. [29] investigated the hydrogen-trapping characteristics of TiC particles in steel and found that the coherence of precipitates/ferrite

is an important factor affecting the hydrogen-trapping capacity of precipitates. Coherent and semi-coherent TiC particles can trap hydrogen during cathodic charging at room temperature, and the hydrogen trapping site is at the TiC/ferrite interface. The smaller the size of TiC particles, the larger the interface area, and the more hydrogen-trapping sites. Incoherent TiC particles, on the other hand, cannot trap hydrogen during cathodic charging at room temperature. Kawakami et al. [30] calculated the hydrogen trapping energy at different sites of TiC particles in bcc-Fe by ab-initio calculation, thus identifying the hydrogen-trapping site in TiC particles as the TiC/bcc-Fe interface. Furthermore, they validated the experimental results using a three-dimensional atom probe. The work of Kawakami et al. can also prove that the density of irreversible hydrogen traps increases with decreasing TiC precipitate size. Shi et al. [31] investigated the hydrogen trapping features of semi-coherent NbC and found that the misfit dislocation core at the NbC/ α -Fe semi-coherent interface is the hydrogen trapping site, which can also be inferred that the number of irreversible hydrogen traps decreases with the increase in NbC size. Cui et al. [32] investigated the effect of NbC precipitates on the hydrogen diffusion in X80 pipeline steel and found that NbC precipitates in the range of 3–10 nm were the main irreversible hydrogen traps. The experimental steel in this paper is a Ti-Nb microalloyed steel. It can be inferred that the precipitates are carbides of Ti and Nb, and the hydrogen traps of these carbides are located at the precipitates/ferritic interface. As the average size of the precipitates in the experimental steel of the present study increases from 7.5 nm to 12.5 nm, the number of irreversible hydrogen traps gradually decreases, and the precipitates may change from semi-coherent to incoherent, which would lead to a significant decrease in the density of irreversible hydrogen traps due to the inability of the precipitates to trap hydrogen. In the study of Lin et al. [33], due to the large size of the TiC precipitates, ranging from 20 to 50 nm, the precipitates were incoherent, so the amount of trapped hydrogen in the irreversible hydrogen traps was very small, which also confirms that the precipitate size has a significant effect on the number of irreversible hydrogen traps. It can be seen that a large amount of semi-coherent precipitates in the matrix is the key to obtaining good fish-scaling resistance.

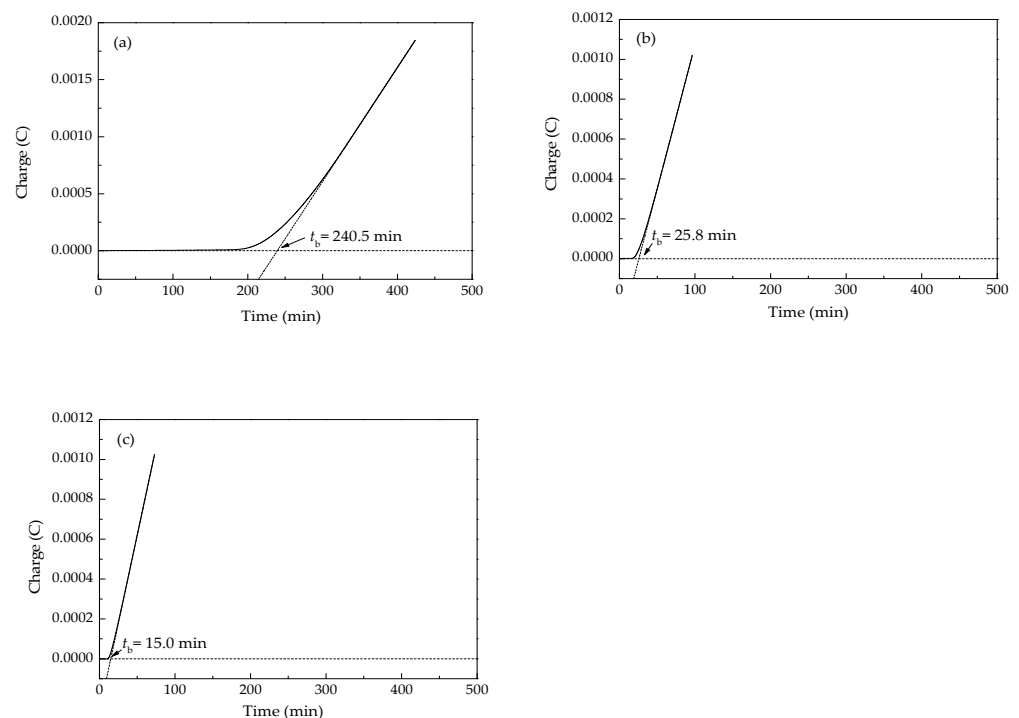


Figure 5. Charge–time curves of hydrogen permeation test: (a) HR sample; (b) EF1 sample; (c) EF2 sample.

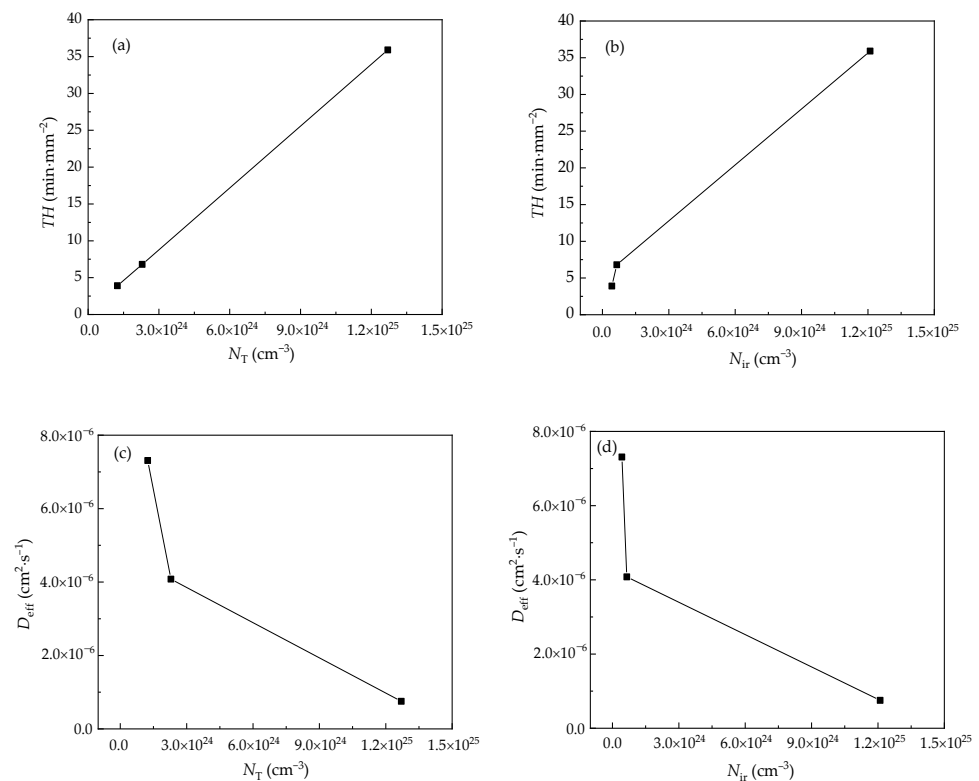


Figure 6. Relationship between TH , D_{eff} , and N_T , N_{ir} : (a) TH – N_T curve; (b) TH – N_{ir} curve; (c) D_{eff} – N_T curve; (d) D_{eff} – N_{ir} curve.

4. Conclusions

In this study, the microstructure, mechanical properties, and fish-scaling resistance of a Ti-Nb microalloyed steel strip and the strips after the first and second simulated enamel firing were investigated. The effect of irreversible hydrogen trap density on fish-scaling resistance was quantitatively investigated by the hydrogen permeation test. The following conclusions were obtained.

(1) The microstructure of the hot-rolled experimental steel is ferrite and fine carbides, with a large number of fine precipitates inside the ferrite grains. The average size of the precipitates is about 7.5 nm. After the first and second enamel firings, the average ferrite grain size increases from 3.21 μm to 5.43 μm and 6.58 μm , and the average size of the precipitates increases to 12.5 nm and 13.5 nm.

(2) The yield strength, tensile strength, and elongation of the hot-rolled experimental steel are 711 MPa, 761 MPa, and 21.0%, respectively. After the first and second enamel firing, the yield strength decreases to 471 MPa and 409 MPa, the tensile strength decreases to 524 MPa and 490 MPa, and the elongation increases to 27.8% and 33.9%.

(3) The TH of the hot-rolled experimental steel is 35.9 min/mm², which is reduced significantly to 6.8 min/mm² after the first enamel firing, and further reduced to 3.9 min/mm² after the second enamel firing. The significant decrease in irreversible hydrogen trap density due to the coarsening of the precipitates is responsible for the significant reduction in the TH . A large number of semi-coherent precipitates in the ferrite matrix is the key to obtaining excellent fish-scaling resistance of hot-rolled enamel steel.

Author Contributions: Methodology, L.D.; formal analysis, Y.Z.; investigation, Y.Z., B.Y. and Y.D.; data curation, Y.Z., B.Y. and Y.D.; writing—original draft preparation, Y.Z.; writing—review and editing, X.W., H.W. and X.G.; supervision, L.D. and J.Z. All authors have read and agreed to the published version of the manuscript.

Funding: This study is funded by the Fundamental Research Funds for the Central Universities (Grant No. N2107013).

Institutional Review Board Statement: Not applicable.

Informed Consent Statement: Not applicable.

Data Availability Statement: Not applicable.

Acknowledgments: The authors acknowledge Yang Zhao and Weina Zhang of Northeastern University for their help in TEM experiments, and the authors also acknowledge Engineer Jin Li of Ma'anshan Iron & Steel Co., Ltd. for their help in hydrogen permeation experiments.

Conflicts of Interest: The authors declare no conflict of interest.

References

1. Nguyen, H.H.; Wan, S.; Tieu, K.A.; Pham, S.T.; Zhu, H. Tribological behaviour of enamel coatings. *Wear* **2019**, *426–427*, 319–329. [[CrossRef](#)]
2. Wang, D. Effect of crystallization on the property of hard enamel coating on steel substrate. *Appl. Surf. Sci.* **2009**, *255*, 4640–4645. [[CrossRef](#)]
3. Liu, M.L.; Tang, H.Q.; Yan, W.; Subramanian, S.V. The effect of the second phase on the anti-scaling property of enamel steel DC04EK. *Metallogr. Microstruct. Anal.* **2022**, *11*, 595–601. [[CrossRef](#)]
4. Huang, X.; Zhang, Z.; Liu, X.; Zhao, Y.; Li, X. Variations of microstructure and resistance to fish-scaling of a hot rolled enamel steel before and after enamel firing. *J. Mater. Res. Technol.* **2021**, *11*, 466–473. [[CrossRef](#)]
5. Zhao, Y.; Huang, X.; Yu, B.; Yuan, X.; Liu, X. Effect of coiling temperature on microstructure, properties and resistance to fish-scaling of hot rolled enamel steel. *Materials* **2017**, *10*, 1012. [[CrossRef](#)]
6. Yang, X.; Jha, A.; Brydson, R.; Cochrane, R.C. The effects of a nickel oxide precoat on the gas bubble structure and fish-scaling resistance in vitreous enamels. *Mater. Sci. Eng. A* **2004**, *366*, 254–261. [[CrossRef](#)]
7. Yang, X.; Jha, A.; Brydson, R.; Cochrane, R.C. An analysis of the microstructure and interfacial chemistry of steel–enamel interface. *Thin Solid Film.* **2003**, *443*, 33–45. [[CrossRef](#)]
8. Liu, Z.; Li, W.; Shao, X.; Kang, Y.; Li, Y. An ultra-low-carbon steel with outstanding fish-scaling resistance and cold formability for enameling applications. *Metall. Mater. Trans. A* **2019**, *50*, 1805–1815. [[CrossRef](#)]
9. Dong, F.; Du, L.; Liu, X.; Xue, F. Optimization of chemical compositions in low-carbon Al-killed enamel steel produced by ultra-fast continuous annealing. *Mater. Charact.* **2013**, *84*, 81–87. [[CrossRef](#)]
10. Liu, Z.; Kang, Y.; Zhang, Z.; Shao, X. Effect of batch annealing temperature on microstructure and resistance to fish scaling of ultra-low carbon enamel steel. *Metals* **2017**, *7*, 51. [[CrossRef](#)]
11. Fang, J.; Xu, C.; Li, Y.; Peng, R.; Fu, X. Effect of grain orientation and interface coherency on the hydrogen trapping ability of TiC precipitates in a ferritic steel. *Mater. Lett.* **2022**, *308*, 131281. [[CrossRef](#)]
12. Takahashi, J.; Kawakami, K.; Kobayashi, Y.; Tarui, T. The first direct observation of hydrogen trapping sites in TiC precipitation-hardening steel through atom probe tomography. *Scr. Mater.* **2010**, *63*, 261–264. [[CrossRef](#)]
13. Wallaert, E.; Depover, T.; Arafim, M.; Verbeken, K. Thermal desorption spectroscopy evaluation of the hydrogen-trapping capacity of NbC and NbN precipitates. *Metall. Mater. Trans. A* **2014**, *45*, 2412–2420. [[CrossRef](#)]
14. Chen, Y.S.; Lu, H.; Liang, J.; Rosenthal, A.; Liu, H.; Sneddon, G.; McCarroll, I.; Zhao, Z.; Li, W.; Guo, A.; et al. Observation of hydrogen trapping at dislocations, grain boundaries, and precipitates. *Science* **2020**, *367*, 171–175. [[CrossRef](#)] [[PubMed](#)]
15. Shi, R.; Chen, L.; Wang, Z.; Yang, X.S.; Qiao, L.; Pang, X. Quantitative investigation on deep hydrogen trapping in tempered martensitic steel. *J. Alloys Compd.* **2021**, *854*, 157218. [[CrossRef](#)]
16. Wei, F.G.; Hara, T.; Tsuchida, T.; Tsuzaki, K. Hydrogen trapping in quenched and tempered 0.42C-0.30Ti steel containing bimodally dispersed TiC particles. *ISIJ Int.* **2003**, *43*, 539–547. [[CrossRef](#)]
17. Ma, Y.; Shi, Y.; Wang, H.; Mi, Z.; Liu, Z.; Gao, L.; Yan, Y.; Su, Y.; Qiao, L. A first-principles study on the hydrogen trap characteristics of coherent nano-precipitates in α -Fe. *Int. J. Hydrogen Energy* **2020**, *45*, 27941–27949. [[CrossRef](#)]
18. Takahashi, J.; Kawakami, K.; Kobayashi, Y. Origin of hydrogen trapping site in vanadium carbide precipitation strengthening steel. *Acta Mater.* **2018**, *153*, 193–204. [[CrossRef](#)]
19. Turk, A.; Martín, D.S.; Rivera-Díaz-del-Castillo, P.E.J.; Galindo-Nava, E.I. Correlation between vanadium carbide size and hydrogen trapping in ferritic steel. *Scr. Mater.* **2018**, *152*, 112–116. [[CrossRef](#)]
20. Wei, F.G.; Tsuzaki, K. *Gaseous Hydrogen Embrittlement of Materials in Energy Technologies*, 1st ed.; Woodhead Publishing Limited: Oxford, UK, 2012; pp. 493–525.
21. Zhou, P.; Li, W.; Zhao, H.; Jin, X. Role of microstructure on electrochemical hydrogen permeation properties in advanced high strength steels. *Int. J. Hydrogen Energy* **2018**, *43*, 10905–10914. [[CrossRef](#)]
22. Devanathan, M.A.V.; Stachurski, Z. The adsorption and diffusion of electrolytic hydrogen in palladium. *Proc. R. Soc. A* **1962**, *270*, 90–102.
23. Samanta, S.; Kumari, P.; Mondal, K.; Dutta, M.; Singh, S.B. An alternative and comprehensive approach to estimate trapped hydrogen in steels using electrochemical permeation tests. *Int. J. Hydrogen Energy* **2020**, *45*, 26666–26687. [[CrossRef](#)]
24. Zhang, S.; Fan, E.; Wan, J.; Liu, J.; Huang, Y.; Li, X. Effect of Nb on the hydrogen-induced cracking of high-strength low-alloy steel. *Corros. Sci.* **2018**, *139*, 83–96. [[CrossRef](#)]

25. Dong, C.F.; Liu, Z.Y.; Li, X.G.; Cheng, Y.F. Effects of hydrogen-charging on the susceptibility of X100 pipeline steel to hydrogen-induced cracking. *Int. J. Hydrogen Energy* **2009**, *34*, 9879–9884. [[CrossRef](#)]
26. Zhang, S.; Chen, W.; Huang, F.; Cheng, Y.K.; Li, K.; Hu, Q.; Liu, J. The significant effect of tantalum on the hydrogen-induced cracking of pipeline steel: Morphology, hydrogen permeation, and theoretical studies. *Corros. Sci.* **2022**, *200*, 110213. [[CrossRef](#)]
27. Jiang, M.; Yang, X.; Pan, S.; Krakauer, B.K.; Zhu, M. Correlation between microstructures and yield strength of a high strength enameling steel. *J. Mater. Sci. Technol.* **2012**, *28*, 737–744. [[CrossRef](#)]
28. Okuyamas, T.; Nishimoto, A.; Kurokawa, T. New type cold rolled steel sheet for enamelling produced by the continuous casting method. *Vitr. Enamel* **1990**, *41*, 49–60.
29. Wei, F.G.; Tsuzaki, K. Quantitative analysis on hydrogen trapping of TiC particles in steel. *Metall. Mater. Trans A* **2006**, *37*, 331–353. [[CrossRef](#)]
30. Kawakami, K.; Matsumiya, T. Numerical analysis of hydrogen trap state by TiC and V₄C₃ in bcc-Fe. *ISIJ Int.* **2012**, *52*, 1693–1697. [[CrossRef](#)]
31. Shi, R.; Ma, Y.; Wang, Z.; Gao, L.; Yang, X.S.; Qiao, L.; Pang, X. Atomic-scale investigation of deep hydrogen trapping in NbC/ α -Fe semi-coherent interfaces. *Acta Mater.* **2020**, *200*, 686–698. [[CrossRef](#)]
32. Cui, Q.; Wu, J.; Xie, D.; Wu, X.; Huang, Y.; Li, X. Effect of nanosized NbC precipitates on hydrogen diffusion in X80 pipeline steel. *Materials* **2017**, *10*, 721. [[CrossRef](#)] [[PubMed](#)]
33. Lin, Y.T.; Chiang, L.J.; Lin, Y.C.; Yen, H.W. New approaches in understanding the effects of hydrogen trapping and the fishscaling resistance of enameled steels. *Surf. Coat. Technol.* **2020**, *399*, 126135. [[CrossRef](#)]